JACS
JOURNAL OF THE AMERICAN CHEMICAL SOCIETY

Article

pubs.acs.org/JACS

Equivalent Circuits of a Self-Assembled Monolayer-Based Tunnel Junction Determined by Impedance Spectroscopy

C. S. Suchand Sangeeth,[†] Albert Wan,[†] and Christian A. Nijhuis*[,†,‡]

[†]Department of Chemistry, National University of Singapore, 3 Science Drive 3, Singapore 117543

[‡]Graphene Research Centre, National University of Singapore, 2 Science Drive 3, Singapore 117542

Supporting Information

ABSTRACT: The electrical characteristics of molecular tunnel junctions are normally determined by DC methods. Using these methods it is difficult to discriminate the contribution of each component of the junctions, e.g., the molecule−electrode contacts, protective layer (if present), or the SAM, to the electrical characteristics of the junctions. Here we show that frequency-dependent AC measurements, impedance spectroscopy, make it possible to separate the contribution of each component from each other. We studied junctions that consist of self-assembled monolayers (SAMs) of *n*-alkanethiolates ($S(CH_2)_{n-1}CH_3 \equiv SC_n$ with n = 8, 10, 12, or 14) of the form Ag^{TS}-SC_n//GaO_x/EGaIn (a protective thin (~0.7 nm) layer of GaO_x forms spontaneously on the surface of EGaIn). The impedance data were fitted to an equivalent circuit consisting of a series resistor (R_S, which includes the SAM-electrode contact resistance), the capacitance of the SAM (C_{SAM}), and the resistance of the SAM (R_{SAM}). A plot of R_{SAM} vs n_C yielded a tunneling decay constant β of 1.03 ± 0.04 n_C^{-1}, which is similar to values determined by DC methods. The value of C_{SAM} is similar to previously reported values, and R_S (2.9−3.6 × 10^{-2} Ω·cm^2) is dominated by the SAM−top contact resistance (and not by the conductive layer of GaO_x) and independent of n_C. Using the values of R_{SAM}, we estimated the resistance per molecule r as a function of n_C, which are similar to values obtained by single molecule experiments. Thus, impedance measurements give detailed information regarding the electrical characteristics of the individual components of SAM-based junctions.

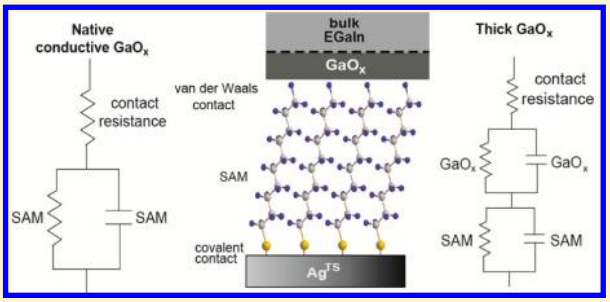

INTRODUCTION

Molecular electronic junctions consist of at least two electrodes and their interfaces with the organic part in the form of single molecules or self-assembled monolayers (SAMs), but the electrical properties measured across SAMs of the same chemical composition, e.g., $S(CH_2)_{n-1}CH_3 \equiv SC_n$, differ greatly across test-beds (see below).[1−3] The nature of the molecule−electrode interface determines, for instance, how the molecular energy levels couple to the electrodes electronically[4−8] and the magnitude of the contact resistance.[9,10] These interfaces may also induce characteristics, such as rectification[11,12] or switching,[13] that are not molecular in origin. Some fabrication methods use a protective layer (PL) between the SAM and the top electrode to avoid damage of the SAM during the fabrication process.[1,14−19] The PL further complicates the interpretation of the electrical characteristics of such junctions. Hence, the roles of the molecule−electrode interfaces and protective barriers, among other factors, such as defects in the electrode material,[20] disorder of the SAMs,[21] or effective electrical contact areas,[3] in the electrical characteristics of the junctions are of great concern but are in general poorly understood.

Figure 1 shows schematically all the components of SAM-based tunnel junctions with, or without, the PL between the SAM and the top electrode. These PLs improve the yields of nonshorting junctions (in some cases even to 100%) and may also provide stability and stop alloy formation with the bottom electrode.[1,15,18,22,23] Studies of charge transport across molecular tunnel junctions are usually conducted by applying a DC voltage V (V) across the junction while measuring the current density J (A/cm^2).[24] These so-called DC measurements are very useful to determine, for instance, the tunneling decay constant β (the rate at which the current decays as a function of the SAM thickness d), or pre-exponential factor J_0 (the current density that would flow across the junction for d = 0 nm), by fitting the charge transport data to a simplified form of the Simmons equation (see eq 8 below).[1−3,16,24,25] But these types of DC measurements only determine the total currents, which are impeded by the total resistance of the junctions, and do not make it possible to separate resistances of the individual components of the junctions, e.g., the interfaces, the SAMs, or protective layers, from each other.[26] In contrast, applying sinusoidal perturbations with a broad range of frequencies while measuring the complex impedance make it possible to separate the individual components of the junctions that have different time domains.[26] The so-called impedance spectroscopy has been widely used to characterize the electrical properties (e.g.,

Received: June 7, 2014

   dx.doi.org/10.1021/ja505420c | J. Am. Chem. Soc. XXXX, XXX, XXX−XXX

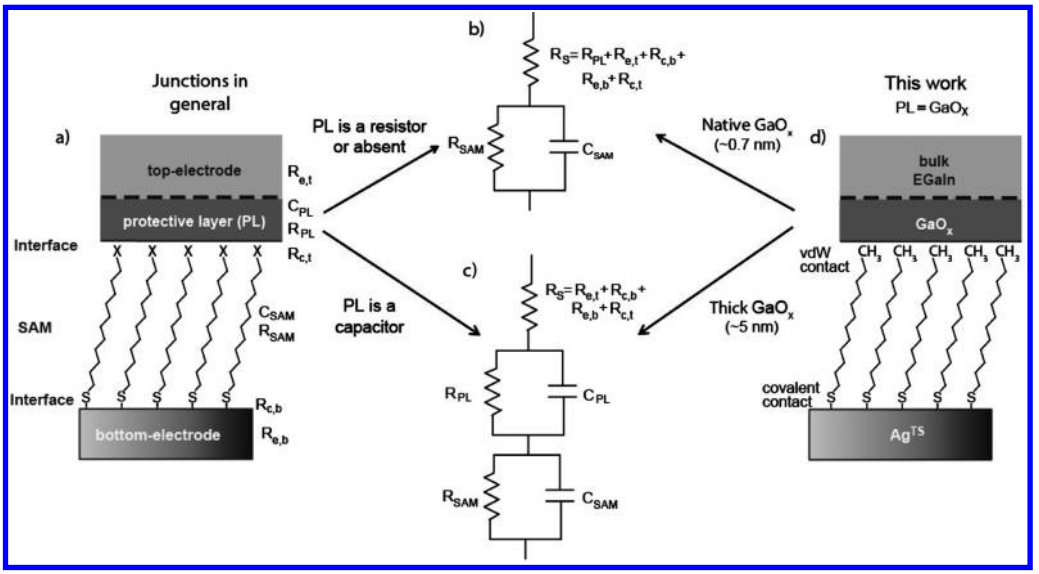

Figure 1. (a) A schematic illustration of a SAM-based tunnel junction with vdW = van der Waals, R_{PL} = the resistance of the protective layer, $R_{c,t}$ = the resistance of the SAM−top electrode interface, R_{SAM} = the resistance of the SAM, $R_{c,b}$ = the resistance of the SAM−bottom electrode interface, C_{SAM} = capacitance of the SAM, and C_{PL} = capacitance of the protective layer. $R_{e,t}$ and $R_{e,b}$ are the resistances caused by the wires, probes, etc. (b) The equivalent circuit for junctions without protective layers, or when the protective layer is a resistor. (c) The equivalent circuit for junctions when the protective layer is a capacitor. (d) A schematic illustration of Ag^{TS}-SC_{12}//GaO_x/EGaIn junction.

ionic and electrical conductivities, capacitances, or interfacial resistances) of various devices including fuel cells,[27−29] organic light emitting diodes,[30] organic field effect transistors,[31−33] and memory devices.[34] This method makes it possible to describe the system in terms of equivalent circuits and to separate, for instance, the resistance of the organic film and contact resistance in thin film devices.[31−37] So far impedance spectroscopy has been rarely used to probe SAM-based junctions and has been mainly used to determine the dielectric constant of the SAM.[38,39]

This paper describes the electrical characterization of junctions of the form of Ag^{TS}-SC_n//GaO_x/EGaIn with n = 8, 10, 12, or 14 by impedance spectroscopy at zero bias by applying a 100 mV sinusoidal perturbation in the frequency range of 100 Hz to 1 MHz in combination with J(V) measurements in the bias range of ±0.50 V. This approach allowed us to measure the contact resistance of the SAM with the top electrode ($R_{c,t}$), the resistance of the SAM (R_{SAM}), the capacitance of the SAM (C_{SAM}), and to estimate the resistance of the oxide layer (R_{GaO_x}). In our junctions, the GaO_x layer is the PL and $R_{PL} = R_{GaO_x}$ applies. Our results show that the native GaO_x layer of 0.7 nm forms an Ohmic contact with the SAMs and has a resistance (5.8×10^{-4} Ω·cm^2) that is roughly 2 orders of magnitude lower than the contact resistance ($2.9-3.6 \times 10^{-2}$ Ω·cm^2). The oxide layer becomes important and dominates the electrical characteristics when its thickness was intentionally increased electrochemically to roughly 5 nm prior to junction fabrication: this thick layer of GaO_x forms a non-Ohmic contact with a resistance that is comparable to that of a SAM of SC_{14}.

The values of J_0, or, in terms of resistance R_0 (see eq 9 below), differ across test-beds by 12 orders of magnitude.[1−3] It has been experimentally observed that the resistance per molecule, r, decreases with increasing number of molecules in the junctions, but the origins of this relation are not fully understood because all factors that contribute to J_0 (or R_0) for a given test-bed are not clear.[1] Comparison across test-beds is further complicated because J_0 or R_0 values are often reported at different applied biases while these are bias-dependent. Thus, it is important to report these values determined at, or around, zero applied bias unless their bias dependence has been established.

The following contributors to J_0 have been identified. We showed that defects in SAM-based junctions can lower, or increase, the value of J_0 over 2−3 orders of magnitude.[20,40] Simeone et al. found that the difference in the effective electrical, A_{elec} (in μm^2), and geometrical area, A_{geo} (in μm^2), is important and result in an underestimation of J_0 by a factor of 10^4 for "EGaIn"-based junctions.[3] Here we show that the contact resistance lowers the apparent value of J_0 by a factor of 10^3 for "EGaIn"-based junctions close to zero bias (the value of J_0 is bias-dependent[2]).

Fabrication methods to construct SAM-based junctions can broadly be categorized into two groups: junctions with a PL and junctions without a PL.[1,4] Test-beds that incorporate protective layers (PLs) between the top electrode and the SAM likely underestimate values of J_0 because of the resistance of the PL. To avoid resistive junctions, conductive protective layers have been used in the form of conductive polymers,[16,41] graphene,[15,42] or its derivatives.[43] The role of the PL in the charge transport properties of junctions is unclear, and it is in general not known whether during the fabrication of the PL the SAMs are damaged, or if their supramolecular structure are altered because of exposure to solvents and potential intercalation, or (partial) penetration, of the PL into the SAM.[23,41]

The contact resistance has been a major concern, but it has been challenging to address directly. Frisbie et al.[44,45] and others[46,47] showed that junctions with two chemisorbed molecule−electrode contacts have a one to 2 orders of magnitude lower contact resistance than junctions with one chemisorbed and one physisorbed molecule−electrode contact. Their results indicate the covalent electrode−thiolate interface has a lower resistance than a noncovalent molecule/electrode interface. Whitesides et al. showed that by changing the van der Waals (vdW) contact in Ag-SAM//SAM-Hg junctions to a

dx.doi.org/10.1021/ja505420c | J. Am. Chem. Soc. XXXX, XXX, XXX−XXX

hydrogen bonded contact, the conductance increased by 3 orders of magnitude.[48] Others have investigated different types of binding groups, e.g., amines, or phosphines, to couple the molecules to the electrodes and concluded that the conductivities of the junctions vary one to 2 orders of magnitude.[6,49−53]

To avoid direct metal deposition onto SAMs, and exposure of SAMs to solvents, we,[20,54,55] and others,[18,22,23,56−61] have used GaO_x/EGaIn to form top-contact to SAMs. This method is useful to conduct physical-organic studies of charge transport, but the presence of the GaO_x was always a concern because metal-oxides may dominate the charge transport properties of the junctions.[3,18,23] We estimated the value of resistance per molecule r from R_{SAM} (which is not impaired by the resistances of the contacts or the conductive GaO_x layer) using the correction factor of 10^4 to account for the difference in A_{elec} and A_{geo}, and assuming that lateral charge transport between the molecules in the SAMs is not important. We found that the r is within 1 order of magnitude of those values reported for single molecule junctions. We believe that the results reported here help to reconcile the vast differences in the electrical characteristics (at least for Ag^{TS}-SC_n//GaO_x/EGaIn junctions) determined for similar molecules across different types of junctions.

BACKGROUND

Junctions with GaO_x/EGaIn Top-Electrodes. The method to form electrical contact to SAMs with cone-shaped tips of GaO_x/EGaIn suspended from a syringe mounted on a micromanipulator is convenient for three reasons.[2,23,56] (i) This method makes it possible to form junctions in high yields that are stable and reproducible and generates statistically large numbers of data (500−1000 J(V) scans per day).[3,23] (ii) This method does not damage the SAM and is sensitive enough to perform subtle studies of charge transport across SAMs as a function of chemical and supramolecular structure.[3,23] (iii) This method yields junctions without the use of photolithography or clean room conditions, and is straightforward to setup in an ordinary laboratory.[2,23,56] Recently, we showed that the log-standard deviations and the user-to-user variation can be reduced by stabilizing the GaO_x/EGaIn electrode in a microfluidic device made of polydimethylsiloxanes (PDMS), but this method requires more elaborated fabrication than junctions based on cone-shaped tips of GaO_x/EGaIn.[55] This stabilization also reduced instabilities associated with micromanipulators (such as drift or vibrations) and made it possible to perform J(V) measurements as a function of temperature. Both methods are compatible with template-stripped bottom electrodes which do not need to be patterned. Thus, the bottom electrodes have never been exposed to photoresist and only briefly to the ambient (we template-strip the electrode just before use) to ensure minimal potential contamination.

Electrical Characteristics of Native GaO_x layer. A large range of resistivities of pure crystals of β-Ga_2O_3 in the range of 1 Ω·cm (for crystal grown from Ga_2O_3 dissolved in pure Ga) to 10^{10} Ω·cm (for epitaxial grown thin films on GaAs) have been reported.[62,63] The resistivity of thin (4−400 nm) films of Ga_2O_3 deposited by electron-beam evaporation was reported to be 10^{12}−10^{13} Ω·cm.[64] Gallium oxide is a deep ultraviolet transparent insulator with a band gap of 4.8 eV.[65,66] Defective gallium oxide layers are conductive due to oxygen vacancies. The resistivity of the layer of GaO_x that forms spontaneously in air on the bulk metal GaIn alloy is difficult to measure because of the liquid nature the bulk alloy and its thickness of only 0.7 nm.[59] Initially, an upper bound of the resistance ($\sim 4 \times 10^{-2}$ Ω·cm^2) of the GaO_x surface layer was estimated by using Cu-wires.[23] Recently, Simeone et al. suggested that the resistivity of this layer was overestimated because of the presence of CuO_x on the copper wires that were used to contact the GaO_x layer.[3] They reported a resistance of 3.3×10^{-4} Ω·cm^2 for this GaO_x layer in contact with HOPG.[3]

Impedance Spectroscopy of SAM-Based Junctions. Rampi et al. determined the dielectric constant ε_r of the SC_n SAMs in Hg-drop based junctions of the form Hg-SAM/SAM-Hg. They modeled the junction assuming the equivalent circuit shown in Figure 1b holds.[39] The capacitance measurements were carried out as a function of the thickness of the SAM and they determined the dielectric constant ε_r using eq 1 where d_{SAM} is the distance between the metal surfaces of a capacitor; ε_0 is the permittivity of the free space, and the geometrical area of the capacitor surfaces equals A_{geo}. They found $\varepsilon_r = 2.7 \pm 0.3$ for n-alkanethiol SAMs.[39]

$$C_{SAM} = \varepsilon_0 \varepsilon_r A_{geo}/d_{SAM} \quad (1)$$

Akkerman et al. reported a similar value of 2.09 ± 0.05 for n-alkanedithiol SAMs on gold contacted with a thin layer of conducting polymer poly(3,4-ethylenedioxythiophene):poly(4-styrenesulfonic acid (PEDOT:PSS) as a top electrode.[38]

Figure 1d shows a schematic illustration of the Ag^{TS}-SC_n//GaO_x/EGaIn tunnel junction, which indicates the circuit elements (composed of capacitances C and resistors R), and shows two possible equivalent circuits. All resistors that are in series ($R_{e,t}$, $R_{e,b}$, R_{PL}, and $R_{c,t}$) appear as a single resistor R_S and the junctions can be modeled using the equivalent circuit shown in Figure 1b. In case the PL (here the layer of GaO_x) is not a simple resistor, but a capacitor, the equivalent circuit shown in Figure 1c has to be used. Because the total impedance consists of both real and imaginary parts, equivalent circuits have to be fitted to the impedance data to obtain the value of each component of the circuit. Often it can be challenging to identify the equivalent circuit. Here we only show two simple possible circuits, but more complicated equivalent circuits may apply to other types of junctions. As we show here, our data fit well to these equivalent circuits and the residual plots fall within the noise levels of the experimental error. Here we varied the thickness of the SAMs, and the properties of the protective layer by controlling the thickness of the GaO_x layer electrochemically, to judge the validity of the proposed equivalent circuits outlined in Figure 1.

Role of Capacitance. The capacitance induces a resistance to the AC signal because of the capacitive reactance $X_c = 1/C\omega$; where C is the capacitance and ω (rad/s) is the frequency of the AC signal. An applied bias causes positive charges to accumulate at one side, and negative charges at the other side, of the capacitor resulting in an electric field that impedes charge transport. At high frequencies this build of charge is limited and the capacitor becomes less resistive with increasing frequency. The modulus (|Z|) and phase of the complex impedance (ϕ) of a system are determined by the circuit elements present in the system. Hence the impedance characterization of these devices is essential for a comprehensive understanding of the equivalent circuit in terms of the components of the complex impedance, and can give insight into the charge transport mechanism occurring across the bulk and interfaces.[26]

dx.doi.org/10.1021/ja505420c | J. Am. Chem. Soc. XXXX, XXX, XXX−XXX

Analysis of Complex Impedance Spectra. Impedance is a more general concept than resistance because it takes the phase into account. The complex impedance Z is expressed as[26]

$$Z = Z' + jZ'' \tag{2}$$

where Z' is the real and Z'' is the imaginary part. In polar form the complex impedance is given by

$$Z = |Z|e^{j\phi} \tag{3}$$

where $|Z|$ is the modulus of the impedance and ϕ represents the phase difference between applied AC voltage and the measured current.[26,28]

For a simple network comprising of resistance R_1 and capacitance C_1 connected in parallel, Z is given by[26]

$$\frac{1}{Z} = \left(\frac{1}{R_1} + j\omega C_1\right) \tag{4}$$

which can be separated into real and imaginary parts as

$$Z = \left(\frac{R_1}{1 + j\omega R_1 C_1}\right) = \left(\frac{R_1}{1 + \omega^2 R_1^2 C_1^2}\right) - j\left(\frac{\omega C_1 R_1^2}{1 + \omega^2 R_1^2 C_1^2}\right) \tag{5}$$

Here ω (= $2\pi f$) is the varying frequency in rad/s. In the presence of series resistance R_s, i.e., the equivalent circuit shown in Figure 1b, eq 5 is modified to[26]

$$Z = \left(R_s + \frac{R_1}{1 + \omega^2 R_1^2 C_1^2}\right) - j\left(\frac{\omega C_1 R_1^2}{1 + \omega^2 R_1^2 C_1^2}\right) \tag{6}$$

The value of Z of an equivalent circuit that consists of two parallel RC components and a series resistance R_s, i.e., the equivalent circuit shown in Figure 1c, is given by[26]

$$Z = \left(R_s + \frac{R_1}{1 + \omega^2 R_1^2 C_1^2} + \frac{R_2}{1 + \omega^2 R_2^2 C_2^2}\right) - j\left(\frac{\omega C_1 R_1^2}{1 + \omega^2 R_1^2 C_1^2} + \frac{\omega C_2 R_2^2}{1 + \omega^2 R_2^2 C_2^2}\right) \tag{7}$$

We used eqs 6 and 7 to fit our data using complex nonlinear least fitting procedures.[26,28] These models only apply to systems that are in thermodynamic equilibrium (the system is stable and did not change during the experiments) and linear (no harmonics are present). To test if the system fulfills these requirements, and thus that eqs 6 and 7 apply, the data must be Kramers–Kronig (KK) transformable.[26,67] The KK-test also helps to determine the noise levels of the data. Figure S3 (Supporting Information) shows the KK-plots from which we conclude that our system is linear and thermodynamically stable (and that the equations below are applicable).

EXPERIMENTAL DETAILS

The preparation of the bottom electrode, the SAMs, and the junctions, have been reported in detail elsewhere (see Supporting Information for more details).[20,21,54,55]

Electrical Measurements. For charge transport measurements the top electrode was gently placed in contact with an Ag^{TS} bottom electrode that supported the SAMs. A drop of GaO_x/EGaIn present at the inlet of the microchannel is contacted using a tungsten probe with a radius of curvature of 25 μm while the bottom electrode was grounded. The J(V) measurements were carried out using a keithley 6430 source meter and data were acquired using LabVIEW. We used a Wayne Kerr LCR meter (model 43100) with sinusoidal signal of an amplitude of 100 mV (or 50 mV as indicated in the main text) at zero bias and varied the frequency from 100 Hz to 1 MHz, to conduct the impedance measurements. We measured first the J(V) characteristics of the device and only selected those junctions that had their electrical characteristic within one log-standard deviation from the mean values of J for the impedance measurements. See ref 55 for the average J(V) curves. For all measurements we used a A_{geo} of 9.6×10^2 μm^2 except for the junctions with an electrochemically grown layer of GaO_x. To measure the impedance spectra across junctions with this top electrode we used a A_{geo} of 2.82×10^3 μm^2 to increase the geometrical capacitance and to overcome the limitation of the instrument (minimum capacitance which can be measured is ~10 pF).

Estimation of the Resistance of the GaO_x Layer. To estimate the resistance of the GaO_x layer, we measured the J(V) characteristics of HOPG//GaO_x/EGaIn (Figure S1, Supporting Information) following a similar procedure as reported by Simeone et al.[3] We further measured the resistance of HOPG (see Figure S2, Supporting Information) using tungsten probes and subtracted this resistance which includes the resistance of HOPG and test leads from the resistance of HOPG//GaO_x/EGaIn junction to obtain a crude estimate of the resistance of the GaO_x layer.

Electrochemical Oxidation of the GaO_x. The GaO_x/EGaIn confined in the PDMS through-hole was oxidized by using a custom built electrochemical cell (AUTOLAB PGSTAT302N) in a Faraday cage. We secured the top electrode with a Teflon sample holder and immersed it in an aqueous solution of 0.1 M $NaClO_4$ as electrolyte, along with a platinum counter electrode and an Ag/AgCl reference electrode. The GaO_x/EGaIn was used as the working electrode and connected to the instrument through a probe at the outlet of the channel. The height of the electrolyte solution was controlled so that only the GaO_x/EGaIn at the end of the PDMS through-hole, but not the GaO_x/EGaIn at the inlet or outlet of the channel, was submerged in the electrolyte solution. The oxidation of the GaO_x/EGaIn was conducted by applying a bias of 0.20 V for 5.0 s. The I(t) curves during the oxidation process were recorded using the software of NOVA 1.7 (Figure S10, Supporting Information). After oxidation, the top electrode was immersed in deionized water (18.2 MΩ·cm) to remove electrolyte and dried in air.

RESULTS AND DISCUSSION

***J*(V) Characteristics.** We formed junctions that incorporated SAMs of SC_n (n = 8, 10, 12, 14) of the form of Ag^{TS}-SC_n//GaO_x/EGaIn following a previously reported procedure (see Supporting Information).[55] Figure 2 shows the junction schematically. We used GaO_x/EGaIn top electrodes stabilized in a through-hole made in a transparent rubber of PDMS for two reasons: these junctions are mechanically more stable than junctions formed with cone-shaped tips of GaO_x/EGaIn suspended from a syringe mounted on a micromanipulator, and the geometrical contact area can be precisely controlled; this control over the geometrical contact area is important to determine the dielectric constant accurately.[55] The geometrical contact area of the top-contact with the SAM was 9.6×10^2 μm^2 (see Figure S9, Supporting Information), which is larger than the typical junction area of $3–5 \times 10^2$ μm^2 obtained with cone-shaped GaO_x/EGaIn electrode for the following two reasons: to enhance the geometrical capacitance of the junction so that it could be measured using our LCR meter, and to reduce the resistance of the junction by increasing the number of molecules in the junction to overcome the limitation of our instrument (input impedance of ~100 MΩ) for high resistance measurements.

Before we started the impedance measurements, we determined the J(V) characteristics of the devices and recorded the values of J over the range of biases of −0.50 to 0.50 V (one trace ≡ 0 V → 0.50 V → −0.50 V → 0 V) at intervals of 20 mV.

dx.doi.org/10.1021/ja505420c | J. Am. Chem. Soc. XXXX, XXX, XXX–XXX

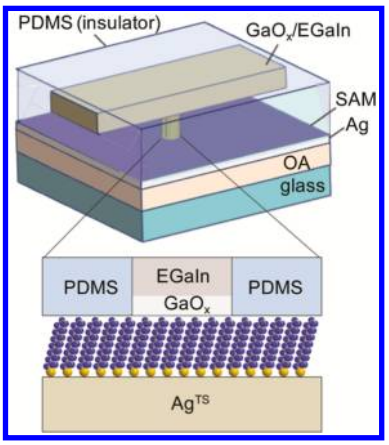

Figure 2. A schematic illustration of the SAM-based junctions (not drawn to scale). The liquid-metal forms stable structures in microchannels in PDMS. The top electrode is encapsulated by the insulating-PDMS and the diameter of the hole determines the geometrical contact area. The bottom electrode is Ag^{TS} (here we used an optical adhesive (OA) and a glass support to strip the Ag off a Si/SiO$_2$ wafer).

We measured a total of 10 J(V) traces for each type of junction and only used devices that had their electrical characteristics within one log-standard deviation from the average values of J of previously reported data. Figure 3a shows the J(V) data (the arithmetic mean of the 10 J(V) curves; the error bars represent the standard deviations) of the junctions we used here to determine the impedance spectra. Figure 3b shows the plot of |J| at −0.50 V vs n_C and that the values of |J| decrease exponentially with increasing n_C. We found β = 1.00 ± 0.06 n_C^{-1} and J_0 = 330 ± 2 A/cm^2 by fitting the data to the simplified Simmons equation (eq 8), which are very close to previously reported data for these junctions (the error bars represent errors from the fits).[55] Thus, we conclude that these junctions represent Ag^{TS}-SC$_n$//GaO$_x$/EGaIn junctions very well.

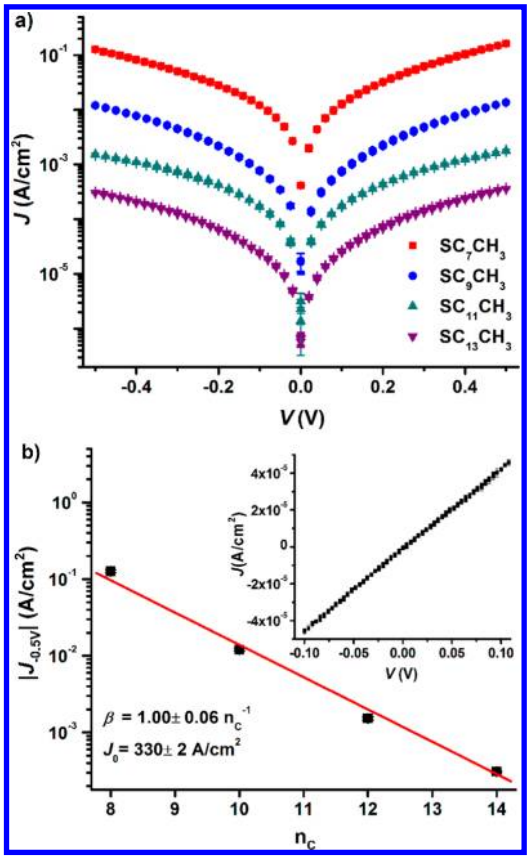

Figure 3. (a) The J(V) characteristics of the Ag^{TS}-SC$_n$//GaO$_x$/EGaIn junctions with n = 8, 10, 12, or 14. (b) The value of |J| as a function of n_C measured at −0.50 V. The red line is a fit to the data using eq 8. Inset shows the current density vs voltage of the Ag^{TS}-SC$_{10}$//GaO$_x$/EGaIn junction in the low bias regime (−0.10 to 0.10 V).

$$J = J_0 e^{-\beta d} \tag{8}$$

Impedance Spectroscopy. The impedance measurements on Ag^{TS}-SC$_n$//GaO$_x$/EGaIn junctions were carried out in the frequency range of 100 Hz to 1 MHz using a sinusoidal signal with an amplitude of 100 mV at zero applied bias (the relatively large amplitude improved the signal-to-noise ratios but did not affect the linearity of the data; see below). Figure 4 shows the frequency dependency of the modulus of the complex impedance (|Z|), phase angle (ϕ), and Nyquist plots. This Figure shows that |Z| increases with molecular chain length as the tunneling distance increases. The frequency dependence of |Z| is nearly constant at low frequencies (dominated by the resistance of the SAM), but it decreases with increasing frequency above the so-called transition frequency f_T (Hz). The f_T is defined as the frequency at which |Z| drops by 10% because the capacitive reactance decreases with frequency (see Background).[68] This value of f_T shifts to higher frequencies as the length of the molecule decreases, because the resistance of the SAM decreases. The value of f_T defines the limitations and requirements of impedance measurements on SAMs which was in our case limited to junctions with n = 8 below which f_T was too large, or n = 14, above which f_T was too small, to be measurable accurately with our setup for junctions with a geometrical area of 9.6 × 10^2 μm^2.[38] The phase is 90° for an ideal capacitor and appears in the Nyquist plot as a semicircle. The phase spectra (Figure 4b) and Nyquist plot (Figures 4c and d) show only a single peak and one semicircle, respectively. This implies the presence of one capacitor. At high frequencies the impedance will saturate to R_S. These features are consistent with an equivalent circuit shown in Figure 1b.

Before we fitted the data to equivalent circuits, we determined the quality of the data with the so-called Kramers−Kronig (KK) test.[26,28,67] Figure S3 (Supporting Information) shows the residual plots of the KK-test and that the data were KK-transformable with values of χ^2_{KK} in the range of 0.0009−0.0027 from which we conclude that the system was stable and did not change during the experiments (the system is in thermodynamic equilibrium) and linear with acceptable signal-to-noise ratios. Indeed, it is well-known that tunnel junctions are linear in the low bias regime (see Figure 3b for the linear J(V) curve of Ag^{TS}-SC$_{10}$//GaO$_x$/EGaIn junction in the bias range of ±0.10 V). In addition, Figure S7 and Table S2 (Supporting Information) show that the impedance data recorded on the same junction but using a 50 or 100 mV perturbation yielded indistinguishable data within experimental error. These results indicate that eqs 6 and 7 are applicable and that the relatively large amplitude of the sinusoidal signal of 100 mV did not cause deviations of the data from linearity.

We fitted the impedance data to the equivalent circuit shown in Figure 1b using complex nonlinear least-squares fitting.[26,28]

dx.doi.org/10.1021/ja505420c | J. Am. Chem. Soc. XXXX, XXX, XXX−XXX

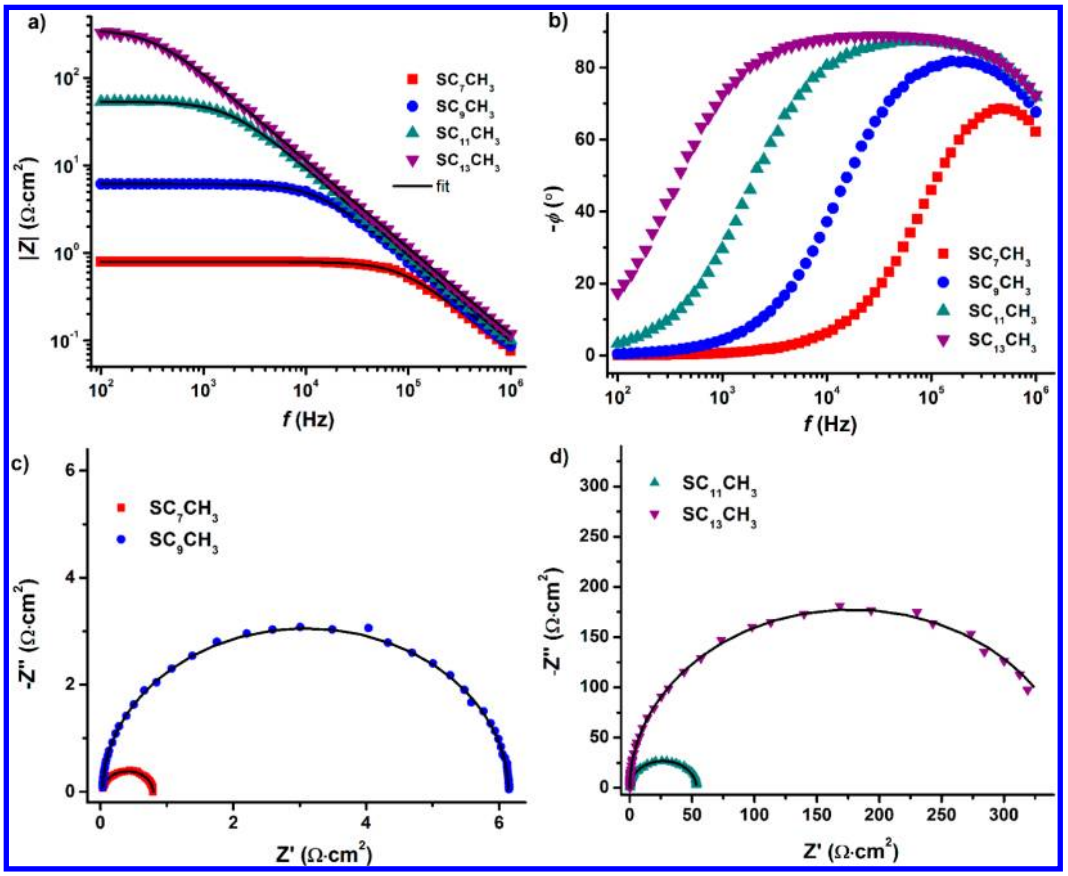

Figure 4. (a) Frequency dependency of |Z| of the junctions at zero bias as a function of n, and (b) the corresponding phase angle vs frequency plots. Nyquist plots of the junctions as a function for n = 8 and 10 (c), and n = 12 and 14 (d). The black lines are fits to the data using eq 6 corresponding to the equivalent circuit shown in Figure 1b.

Table 1. Results of the Fits of the Equivalent Circuits to the Impedance Data[a]

SAM	d_{GaO_x} (nm)	R_{SAM} (Ω·cm²)	C_{SAM} (μF/cm²)	R_{PL} (Ω·cm²)	C_{PL} (μF/cm²)	R_S (× 10^{-2} Ω·cm²)
SC_7CH_3[b]	0.7	0.73 ± 0.04	2.44 ± 0.12			2.9 ± 0.2
SC_9CH_3[b]	0.7	5.8 ± 0.4	2.06 ± 0.10			3.2 ± 0.3
$SC_{11}CH_3$[b]	0.7	51 ± 2	1.76 ± 0.09			3.0 ± 0.3
$SC_{13}CH_3$[b]	0.7	339 ± 19	1.47 ± 0.07			3.6 ± 0.4
SC_9CH_3[c,e]	5.2[d]	7.8 ± 0.5	2.31 ± 0.12	626 ± 33	0.61 ± 0.07	5.9 ± 0.6
SC_9CH_3[b,e]	0.7	7.5 ± 0.4	2.16 ± 0.10			2.9 ± 0.3

[a]The error bars represent the error from the fit to the corresponding equivalent circuits. [b]Data obtained by fitting to the equivalent circuit shown in Figure 1b. [c]Data obtained by fitting to the equivalent circuit shown in Figure 1c. [d]Determined from the measured value of C_{GaO_x}. [e]These data were recorded with a geometrical junction area of 2.82 × 10^3 μm².

The equivalent circuit fits well to our data (see residual plots Figure S4, Supporting Information), and the error of the fits (χ^2_{Fit} ranges from 0.0012 to 0.0036) are similar to the χ^2_{KK} values, which we attribute to noise. Table 1 summarizes the fitting parameters.

Resistance and Capacitance of the SAM. The simplified Simmons equation for current density (eq 8) can be modified to relate the thickness of the SAM to the resistance of the junction using eq 9a, where R_0 is the hypothetical resistance across the junction for d = 0 nm.[44] Here we determined R_{SAM} directly and thus eq 9b applies. Although both equations yield very similar values of β, eq 9b gives $R_{SAM,0}$ which is independent of the contact resistances, resistances caused by the PL, i.e., the native layer of GaO_x, or capacitances (see Figure 1). Often R_0 is determined at an arbitrary chosen bias while the factors that contribute to R_0, e.g., the resistance of SAM/electrode contact, or the resistance of the PL, may depend on the applied bias differently. The value of $R_{SAM,0}$ is determined around zero applied bias and does not suffer from these ambiguities. (See below for details regarding eq 9c.)

$$R = R_0 e^{\beta d} \tag{9a}$$

$$R_{SAM} = R_{SAM,0} e^{\beta d} \tag{9b}$$

$$r = r_0 e^{\beta d} \tag{9c}$$

Figure 5a shows the fit of eq 9b to R_{SAM} as a function of n_C which gives a value of β = 1.03 ± 0.04 n_C^{-1} and $R_{SAM,0}$ = 1.9 ± 0.3 × 10^{-4} Ω·cm² (the error represents the mean square deviation obtained from the least-squares fitting procedure). This value of β is very close to previously reported values and falls in the range of consensus value of 0.90−1.1 n_C^{-1}.[2,55]

dx.doi.org/10.1021/ja505420c | J. Am. Chem. Soc. XXXX, XXX, XXX−XXX

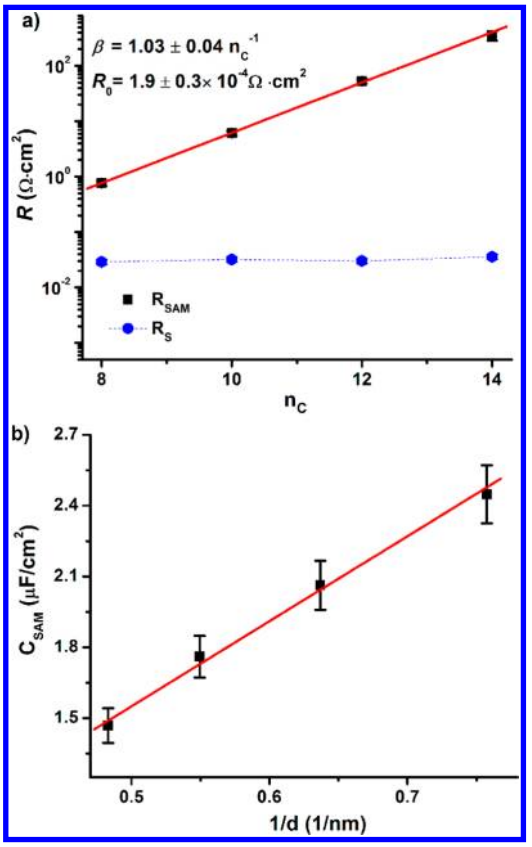

Figure 5. a) The value of R_{SAM} (black squares) and R_S (blue dots) vs n_C. The red solid line is a fit to eq 9b, and the dashed blue line serves only as a guide to the eye. (b) The value of C_{SAM} vs $1/d$ (black squares) with a fit (red solid line) to eq 1.

Figure 5b shows the linear dependence of C_{SAM} as a function of $1/d$ as expected for a parallel plate capacitor (eq 1). The capacitance depends on A_{geo}, but as discussed in the Background section, the effective electrical contact area A_{elec} and the value of A_{geo} differs by 4 orders of magnitude.[3] We estimated the value of ε_r by fitting the data to eq 1 using A_{geo} and found that $\varepsilon_r = 3.4 \pm 0.4$. This value is in good agreement with a previously reported value 2.7 ± 0.3 for Hg-drop junctions[39] (both values are larger than the value of 2.09 ± 0.05 determined by PEDOT:PSS junctions),[38] from which we conclude that the capacitance, unlike the resistance of the SAM (see below), is mainly determined by A_{geo} but not by the effective electrical contact area.

The value of R_S is independent of the thickness of the SAM (or the value of n; Figure 5a). As discussed below, we believe that this value is dominated by the contact resistance of the noncovalent contact of the top electrode with the SAM. The observation that R_S is constant indicates that variations in the SAM//GaO_x/EGaIn from junction-to-junction are insignificant. From these results we conclude that the equivalent circuit shown in Figure 1b describes our junctions accurately.

Contact Resistance. As mentioned above, the resistance R_S is the sum of all resistances in the circuit that are in series (Figure 1). We hypothesize that the value of R_S is dominated by the resistance of the noncovalent contact between the GaO_x layer and the SAM ($R_{c,t}$). To prove our hypothesis, we determined the values R_S, and R_{GaO_x} (here $R_{PL} = R_{GaO_x}$) using DC methods as follows. To characterize our system, we determined the resistance of the two tungsten contact probes and their test-leads by measuring the resistance of HOPG using the same setup we used for the impedance measurements over the bias range of ±0.50 V. This measurement resulted in linear $J(V)$ curves with a resistance of 6.3×10^{-5} Ω·cm^2 (Figure S2, Supporting Information). We repeated this measurement but now with a drop of EGaIn with its surface layer of GaO_x on HOPG with one probe in contact with HOPG and the other in contact with bulk EGaIn. From the linear $J(V)$ curve we derived a resistance for the junction of HOPG//GaO_x/EGaIn of 6.4×10^{-4} Ω·cm^2. The resistance of the native GaO_x layer roughly equals $6.4 \times 10^{-4} - 6.3 \times 10^{-5} = 5.8 \times 10^{-4}$ Ω·cm^2, which is close to the much more precisely determined value of 3.3×10^{-4} Ω·cm^2 reported by Simeone et al.[3] As mentioned in the Introduction, the resistance of metal−thiolate interface is 1−2 orders of magnitude smaller than the physisorbed metal/molecule contact due to the covalent character and polarizablitity of the metal−thiolate bond.[44−47]

The experimentally determined value of R_S is the sum of all resistors of the junction that are in series and is given by eq 10 (all symbols are defined in Figure 1).

$$R_S = R_{e,t} + R_{e,b} + R_{c,b} + R_{c,t} + R_{GaO_x} \quad (10)$$

The value of R_S is independent of the thickness of the SAM or GaO_x and has a value of $2.9-3.6 \times 10^{-2}$ Ω·cm^2 (Table 1 and Figure 5). We did not measure all individual values of $R_{e,t}$, $R_{e,b}$, and $R_{c,b}$, but these values, and R_{GaO_x} of the native layer of GaO_x, are all roughly 2 orders of magnitude smaller than R_S. Thus, we conclude that the value of R_S is mainly determined by the van der Waals contact $R_{c,t}$ and the assumption that $R_S = R_{c,t}$ only introduces a very small error (~2%) in the interpretation of the data.

Resistance Per Molecule. The SAM-based junctions contain large number of molecules in parallel contacted by the two electrodes. Assuming that the resistances of all the molecules are the same and that no lateral charge transfer occurs between the molecules in the SAM, the total resistance of the SAM can be defined by eq 11 where n_{mol} is the number of molecules in the junctions which is determined by the surface coverage of the SAM, Γ_{SAM}, (in molecules/cm^2), and r is the resistance of a single molecule.

$$1/R_{SAM} = 1/r+1/r+1/r+\cdots = n_{mol}/r = \Gamma_{SAM}/r \quad (11)$$

For SAMs of SC_n on gold, Γ_{SAM} is ~4.5×10^{14} molecules/cm^2,[69] from which we estimate the number of molecules in our junctions to be 4.3×10^9. We estimated the resistance per molecule r using R_{SAM} and eq 11 while assuming that $A_{elec} = A_{geo}$. Figure 6 shows r as a function of n_C. Figure 6 also shows the previously reported values of r in junctions with alkanethiols or alkanedithiols measured using conductive probe atomic force microscopy (CP-AFM) or scanning tunneling microscopy (STM) break-junctions, respectively.[44,53,70,71] The single molecule resistance of junctions with alkanedithiols is one to two orders smaller than that of junctions with alkanethiols due the presence of two chemisorbed molecule−electrode contacts in former, whereas the latter consist of one chemisorbed and one physisorded molecule−electrode contact.[44] We found that the resistance r are a factor of 10^4-10^5 higher than values of r estimated by single molecules experiments.[3]

The estimated resistance per molecule depends on the number of molecules contributing to the charge conduction in the junction. The A_{elec} area is a key factor in determining the

dx.doi.org/10.1021/ja505420c | J. Am. Chem. Soc. XXXX, XXX, XXX−XXX

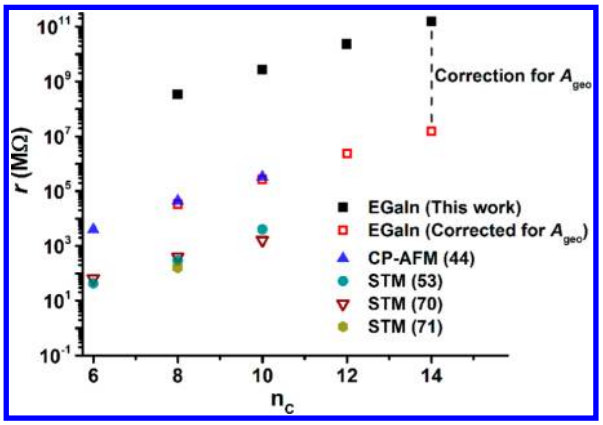

Figure 6. A semilog plot of the resistance per molecule (r) obtained in different experimental test-beds as a function of n_C (with the references given in the parentheses). Error bars are omitted for clarity. The STM break junction experiments[53,70,71] were conducted using alkanedithiolate SAMs.

number of molecules taking part in electrical conduction. Consequently, assuming $A_{geo} = A_{elec}$ leads to a significant overestimation of the electrical contact area and thereby an overestimation of the value of r. Simeone et al. showed that the effective electrical contact area is much smaller ($\sim 10^{-4}$ times) than the geometrical contact area for Ag^{TS}-SC_n//GaO_x/EGaIn junctions.[3] Figure 6 shows the resistance per molecule corrected for A_{elec} as a function of n_C. If we use this correction factor, our values of r fall in the range of r values determined in single molecule experiments.[1,3]

Role of the GaO_x Layer. To determine the role of the GaO_x layer on the charge transport characteristics, we formed junctions with a GaO_x/EGaIn top electrode with an electrochemically grown thick layer of GaO_x (abbreviated as GaO_x^{thick}) on the bulk EGaIn which we abbreviate as GaO_x^{thick}/EGaIn (see Experimental Details). Figure 7 shows the J(V) curves for junctions with a SAM of SC_{10} on Ag^{TS} in contact with GaO_x^{thick}/EGaIn or in contact with a native GaO_x/EGaIn electrode. The GaO_x^{thick}/EGaIn junctions show asymmetrical characteristics and rectify currents with a rectification ratio $R \equiv |J|(-2.0\ V)/|J|(+2.0\ V)$ of roughly 58 ± 2. We also observed

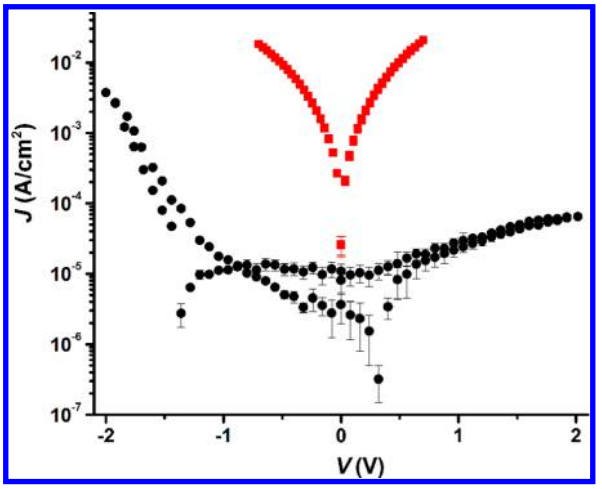

Figure 7. Current density vs applied voltage for junctions with a SAM of SC_9CH_3 on Ag^{TS} using GaO_x^{thick}/ EGaIn top electrode (black) and a native GaO_x/EGaIn top electrode (red).

charging effects at low bias (−1.4 to 0.80 V) which we attribute to charge trapping centers caused by defects (presumably oxygen vacancies). These results stand in sharp contrast with the results obtained for junctions with a native layer of GaO_x; these junctions did not show charging, are not stable at applied biases of > ±1.0 V (but junctions with n = 8 or 10 were only stable up to ±0.7 V) and produce (nearly) symmetrical J(V) curves with R of 0.5−0.8 at ±0.50 V (Figure 3a).[23]

To investigate the properties of the junctions Ag^{TS}-SC_{10}//GaO_x^{thick}/EGaIn in more detail, we recorded impedance spectra. Because of the large resistance of the junctions, we recorded the impedance spectra using junctions with a A_{geo} of $2.82 \times 10^3\ \mu m^2$. Figure 8 shows the Bode and Nyquist plots for the corresponding junction. The modulus of the complex impedance is ∼80 times higher than the impedance of junctions with EGaIn top electrodes with native layers of GaO_x. The phase spectrum shows two peaks (Figure 8b) and the Nyquist plot shows the presence of two semicircles (Figure 8c), which indicate the presence of two capacitances: the capacitive contributions from the thick oxide layer and the SAM.

We fitted the impedance data to the equivalent circuit shown in Figure 1c, and Table 1 summarizes the fitting parameters (the Kramers−Kronig plot and residual plots are given in Figures S5 and S6, Supporting Information, respectively). The values of R_{SAM} and C_{SAM} of the SC_{10} SAM were the same (within the standard deviation; Table 1) as those values determined across a junction with the same value of A_{geo} but with a native GaO_x layer. The resistance of the thick oxide layer $R_{GaO_x,thick} = 6.26 \pm 0.33 \times 10^2\ \Omega \cdot cm^2$ and is similar to the resistance of the SAM of SC_{14}. Using a reported value of the dielectric constant of GaO_x of 3.57,[72] we estimated a thickness of the oxide layer of 5.2 ± 0.2 nm by using eq 1 and capacitance of the thick oxide layer $C_{GaO_x,thick}$ of 0.61 $\mu F/cm^2$ (Table 1). The results indicate that the thick electrochemically grown oxide layer makes the junctions resistive and dominates the charge transport properties. These findings confirm that the native GaO_x layer does not contribute significantly to the electrical characteristics of the junctions and that the proposed equivalent circuit (Figure 1b) describes our junctions well.

Interestingly, the R_S values for both types of junctions with native and an electrochemically grown GaO_x film only differ by a factor of 2 from each other. This observation implies that the SAM//GaO_x contact was not affected and confirms the reproducibility of this contact from junction-to-junction.

■ CONCLUSIONS

Properties of the SAM//GaO_x/EGaIn Contact Are Constant and Reproducible. Impedance measurements allowed us to determine the contact resistance between the GaO_x/EGaIn top electrode and the SAM, which only varied over the range of $2.9-3.6 \times 10^{-2}\ \Omega \cdot cm^2$ for junctions with SAMs of SC_n with n = 8, 10, 12, and 14 (Table 1). Even for a junction with an electrochemically grown GaO_x layer of roughly 5 nm the contact resistance was $5.9 \times 10^{-2}\ \Omega \cdot cm^2$. Although our data only make it possible to estimate the effective electrical contact area of the junctions (which are smaller than the geometrical contact area by about 2−4 orders of magnitude), they agree with a more precisely measured value of 10^4 determined by Simeone et al.[3] For physical-organic studies of charge transport, the exact value of the contact resistance or effective electrical contact areas are not important provided they are constant unless one wishes to compare absolute values

dx.doi.org/10.1021/ja505420c | J. Am. Chem. Soc. XXXX, XXX, XXX−XXX

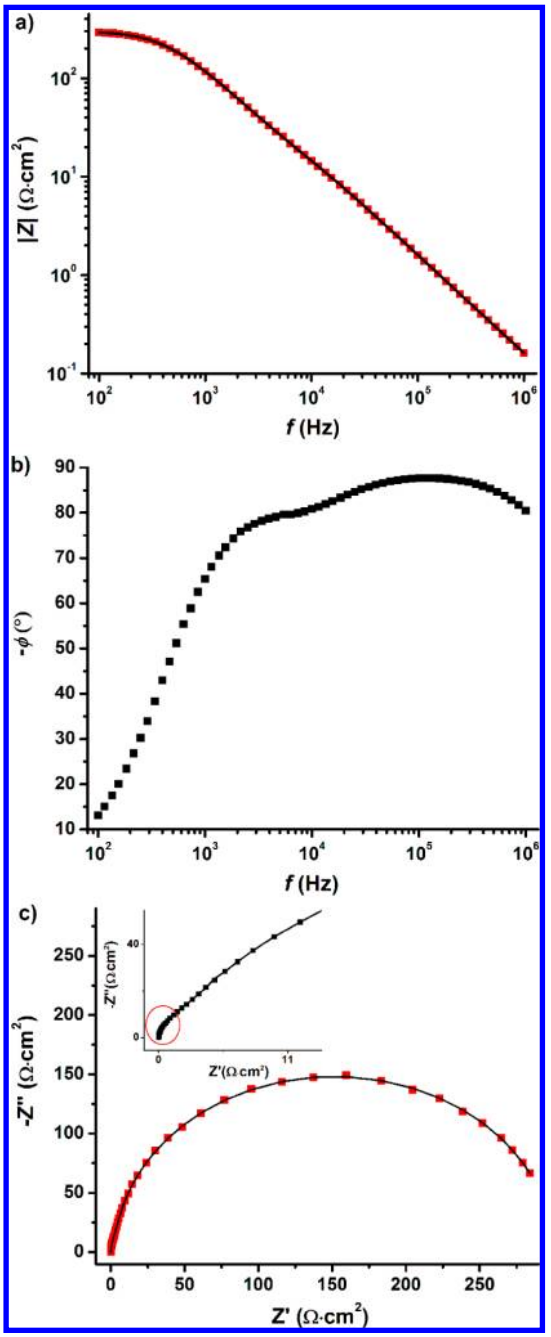

Figure 8. Impedance data for a Ag^{TS}-SC_{10}//GaO_x^{thick}/EGaIn junction: (a) frequency dependence of |Z| and (b) the phase angle, and (c) the Nyquist plot. Inset shows the Nyquist plot with the axes in different scales to show the semicircle at high frequencies. The solid lines represent fits (eq 7) to the equivalent circuit shown in Figure 1c.

across test-beds. From these observations we conclude that the details of the SAM//GaO_x/EGaIn contact are reproducible and that the "EGaIn"-technique is suitable for conducting physical-organic studies of charge transport across SAMs.

Native GaO_x Layer Does Not Significantly Contribute to the Charge Transport Characteristics of Ag^{TS}-SC_n//GaO_x/EGaIn-Based Junctions. The impedance data were fitted to a relatively simple equivalent circuit (Figure 1b) where the resistance of the GaO_x layer, lumped with all other resistances (labeled as R_S) including the resistance of the electrode materials, interfaces, etc., is in series with the resistance and capacitance of the SAM. To deconvolute the contribution of the oxide layer to R_S from other potential factors, we estimated a resistance of the GaO_x layer of 5.8×10^{-4} Ω·cm² which agrees well with a previously reported value of 3.3×10^{-4} Ω·cm² by Simeone et al.[3] We found the R_{GaO_x} is roughly 2 orders of magnitude ($= R_{GaO_x}/R_S$) smaller than R_S. We also used DC methods to estimate the total resistance of the electrode materials, the contact probes, the cables and wires of the probe station, source meter, etc., which all do not contribute significantly to R_S. It has been reported that metal−thiolate interfaces have roughly 1−2 orders of magnitude lower resistances than noncovalent molecule/electrode interfaces.[44−47] For these reasons we believe that the SAM//GaO_x interface (and not the GaO_x) dominates R_S.

Impedance Spectroscopy Makes It Possible to Describe Junctions in Terms of Equivalent Circuits. Normally the properties of SAM-based junctions are probed using DC methods which cannot discriminate between, for instance, the contribution of the SAM from the interfaces, the capacitive from the noncapacitive impedances, or the role of a protective layer (if present), because only the total current that flows across the whole junction is measured as a function of bias. Here we used impedance spectroscopy to determine the components of the junctions that impede charge transport. We found that our junctions can be modeled with a simple model where the resistance of all interfaces and the protective GaO_x layer are in series with the resistance and capacitance of the SAM. Even for a junction where the GaO_x layer thickness was intentionally increased and dominated the J(V) characteristics, i.e., a junction where the protective layer dominates the properties of the junctions, the contributions of this thick layer of GaO_x could be separated from that of the SAM by impedance spectroscopy. We believe that a combination of DC and AC measurements could also be useful to separate nonmolecular effects, e.g., interfaces or protective layers, from molecular effects, in other types of junctions. We plan to perform potentiodynamic impedance measurement in the near future to further validate the proposed equivalent circuits in more detail and to study how the each circuit element depends on the applied bias.

Factors That Dominate the Values R_0, $R_{SAM,0}$, or r Have to Be Identified to Reconcile Differences between Test-Beds. Inherent to the limitation of the simple and convenient procedure of fitting the simplified Simmons equation to a plot of the values of J for a given applied bias as function n_C, the value of the pre-exponential factor J_0 cannot be related straightforwardly to the physical properties of the junctions.[73,74] Indeed, the values of J_0 differ across test-beds by 12 orders of magnitude.[1−3] In addition, J_0 is often reported far away from zero bias and therefore cannot be converted to R_0 straightforwardly complicating comparisons across test beds unless their bias dependence is known. The role of defects[20,40] or PLs, and the effective electrical contact area,[3] are important to understand as each factor can alter the apparent J_0 values by a factor of 10^2−10^4.

Here we show that the resistance of the PL is not important in junctions of Ag^{TS}-SC_n//GaO_x/EGaIn and therefore it does not contribute to the value of J_0 (ignoring it only introduces an error of ∼2% in the contact resistance), but whether this is true for other platforms that use other types of PLs is currently unknown. For Ag^{TS}-SC_n//GaO_x/EGaIn junctions it seems that the value of J_0 is largely dominated by the effective electrical contact area and the noncovalent contact between the SAM

dx.doi.org/10.1021/ja505420c | J. Am. Chem. Soc. XXXX, XXX, XXX−XXX

and the top electrode. Using impedance spectroscopy, we determined R_{SAM} free from contributions of the contact resistances at zero applied bias. From this value we estimated the single molecule resistance which was comparable to values determined by single molecule junctions after we corrected the data for the difference between the effective electrical and geometrical contact areas. Thus, it seems that the large difference in the electrical characteristics between our junctions and that of single molecule junctions can be reconciled using only one correction factor.

■ ASSOCIATED CONTENT

Supporting Information

Additional experimental details, residual and Kramers-Kroning plots, electrical characterization of the HOPG//GaO_x/EGaIn junction, AFM image of the Ag^{TS} electrode, and optical micrographs of the top electrodes. This material is available free of charge via the Internet at http://pubs.acs.org.

■ AUTHOR INFORMATION

Corresponding Author

chmnca@nus.edu.sg

Notes

The authors declare no competing financial interest.

■ ACKNOWLEDGMENTS

The Singapore National Research Foundation (NRF Award No. NRF-RF 2010-03 to C.A.N.) is gratefully acknowledged for supporting this research.

■ REFERENCES

(1) Akkerman, H. B.; de Boer, B. *J. Phys.: Condens. Matter* **2008**, *20*, 1.
(2) Nijhuis, C. A.; Reus, W. F.; Barber, J. R.; Whitesides, G. M. *J. Phys. Chem. C* **2012**, *116*, 14139.
(3) Simeone, F. C.; Yoon, H. J.; Thuo, M. M.; Barber, J. R.; Smith, B.; Whitesides, G. M. *J. Am. Chem. Soc.* **2013**, *135*, 18131.
(4) Moth-Poulsen, K.; Bjornholm, T. *Nat. Nanotechnol.* **2009**, *4*, 551.
(5) Haick, H.; Cahen, D. *Prog. Surf. Sci.* **2008**, *83*, 217.
(6) Park, Y. S.; Whalley, A. C.; Kamenetska, M.; Steigerwald, M. L.; Hybertsen, M. S.; Nuckolls, C.; Venkataraman, L. *J. Am. Chem. Soc.* **2007**, *129*, 15768.
(7) Lindsay, S. M.; Ratner, M. A. *Adv. Mater.* **2007**, *19*, 23.
(8) Sotthewes, K.; Geskin, V.; Heimbuch, R.; Kumar, A.; Zandvliet, H. J. W. *APL Mater.* **2014**, *2*, 010701.
(9) Kim, B.; Choi, S. H.; Zhu, X. Y.; Frisbie, C. D. *J. Am. Chem. Soc.* **2011**, *133*, 19864.
(10) Ricœur, G.; Lenfant, S.; Guérin, D.; Vuillaume, D. *J. Phys. Chem. C* **2012**, *116*, 20722.
(11) McCreery, R.; Dieringer, J.; Solak, A. O.; Snyder, B.; Nowak, A. M.; McGovern, W. R.; DuVall, S. *J. Am. Chem. Soc.* **2003**, *125*, 10748.
(12) Salomon, A.; Boecking, T.; Chan, C. K.; Amy, F.; Girshevitz, O.; Cahen, D.; Kahn, A. *Phys. Rev. Lett.* **2005**, *95*, 266807.
(13) Stewart, D. R.; Ohlberg, D. A. A.; Beck, P. A.; Chen, Y.; Williams, R. S.; Jeppesen, J. O.; Nielsen, K. A.; Stoddart, J. F. *Nano Lett.* **2003**, *4*, 133.
(14) Haick, H.; Cahen, D. *Acc. Chem. Res.* **2008**, *41*, 359.
(15) Wang, G.; Kim, Y.; Choe, M.; Kim, T. W.; Lee, T. *Adv. Mater.* **2011**, *23*, 755.
(16) Akkerman, H. B.; Blom, P. W. M.; de Leeuw, D. M.; de Boer, B. *Nature* **2006**, *441*, 69.
(17) Slowinski, K.; Fong, H. K. Y.; Majda, M. *J. Am. Chem. Soc.* **1999**, *121*, 7257.
(18) Chiechi, R. C.; Weiss, E. A.; Dickey, M. D.; Whitesides, G. M. *Angew. Chem., Int. Ed.* **2008**, *47*, 142.
(19) Holmlin, R. E.; Haag, R.; Chabinyc, M. L.; Ismagilov, R. F.; Cohen, A. E.; Terfort, A.; Rampi, M. A.; Whitesides, G. M. *J. Am. Chem. Soc.* **2001**, *123*, 5075.
(20) Yuan, L.; Jiang, L.; Zhang, B.; Nijhuis, C. A. *Angew. Chem., Int. Ed.* **2014**, *53*, 3377.
(21) Jiang, L.; Yuan, L.; Cao, L.; Nijhuis, C. A. *J. Am. Chem. Soc.* **2014**, *136*, 1982.
(22) Reus, W. F.; Thuo, M. M.; Shapiro, N. D.; Nijhuis, C. A.; Whitesides, G. M. *ACS Nano* **2012**, *6*, 4806.
(23) Nijhuis, C. A.; Reus, W. F.; Whitesides, G. M. *J. Am. Chem. Soc.* **2009**, *131*, 17814.
(24) Cuevas, J. C.; Scheer, E. *Molecular Electronics: An Introduction to Theory and Experiment*; World Scientific: Singapore, 2010.
(25) Simmons, J. G. *J. Appl. Phys.* **1963**, *34*, 1793.
(26) Macdonald, J. R., Johnson, W. B., Ed.; *Impedance Spectroscopy Theory, Experiment, and Applications*; John Wiley & Sons, Inc.: Hoboken, NJ, 2005; pp 1−27.
(27) Springer, T. E.; Zawodzinski, T. A.; Gottesfeld, S. *J. Electrochem. Soc.* **1991**, *138*, 2334.
(28) Boukamp, B. A. *Solid State Ionics* **1986**, *20*, 31.
(29) Pudmich, G.; Boukamp, B. A.; Gonzalez-Cuenca, M.; Jungen, W.; Zipprich, W.; Tietz, F. *Solid State Ionics* **2000**, *135*, 433.
(30) Campbell, I. H.; Smith, D. L.; Ferraris, J. P. *Appl. Phys. Lett.* **1995**, *66*, 3030.
(31) Sangeeth, C. S. S.; Jaiswal, M.; Menon, R. *Appl. Phys. Lett.* **2009**, *95*, 093308.
(32) Sangeeth, C. S. S.; Stadler, P.; Schaur, S.; Sariciftci, N. S.; Menon, R. *J. Appl. Phys.* **2010**, *108*, 113703.
(33) Jaiswal, M.; Menon, R. *Appl. Phys. Lett.* **2006**, *88*, 123504.
(34) Colle, M.; Buchel, M.; de Leeuw, D. M. *Org. Electron.* **2006**, *7*, 305.
(35) Li, Y.; Gao, J.; Yu, G.; Cao, Y.; Heeger, A. J. *Chem. Phys. Lett.* **1998**, *287*, 83.
(36) Garcia-Belmonte, G.; Munar, A.; Barea, E. M.; Bisquert, J.; Ugarte, I.; Pacios, R. *Org. Electron.* **2008**, *9*, 847.
(37) Glatthaar, M.; Riede, M.; Keegan, N.; Sylvester-Hvid, K.; Zimmermann, B.; Niggemann, M.; Hinsch, A.; Gombert, A. *Sol. Energy Mater. Sol. Cells* **2007**, *91*, 390.
(38) Akkerman, H. B.; Naber, R. C. G.; Jongbloed, B.; van Hal, P. A.; Blom, P. W. M.; de Leeuw, D. M.; de Boer, B. *Proc. Natl. Acad. Sci. U. S. A.* **2007**, *104*, 11161.
(39) Rampi, M. A.; Schueller, O. J. A.; Whitesides, G. M. *Appl. Phys. Lett.* **1998**, *72*, 1781.
(40) Jiang, L.; Sangeeth, C. S. S.; Wan, A.; Vilan, A.; Nijhuis, C. A., unpublished results.
(41) Neuhausen, A. B.; Hosseini, A.; Sulpizio, J. A.; Chidsey, C. E. D.; Goldhaber-Gordon, D. *ACS Nano* **2012**, *6*, 9920.
(42) Seo, S.; Min, M.; Lee, S. M.; Lee, H. *Nat. Commun.* **2013**, *4*, 1920.
(43) Seo, S.; Min, M.; Lee, J.; Lee, T.; Choi, S.-Y.; Lee, H. *Angew. Chem., Int. Ed.* **2012**, *51*, 108.
(44) Engelkes, V. B.; Beebe, J. M.; Frisbie, C. D. *J. Am. Chem. Soc.* **2004**, *126*, 14287.
(45) Beebe, J. M.; Engelkes, V. B.; Miller, L. L.; Frisbie, C. D. *J. Am. Chem. Soc.* **2002**, *124*, 11268.
(46) Kaun, C.-C.; Guo, H. *Nano Lett.* **2003**, *3*, 1521.
(47) Li, X.; He, J.; Hihath, J.; Xu, B.; Lindsay, S. M.; Tao, N. *J. Am. Chem. Soc.* **2006**, *128*, 2135.
(48) Rampi, M. A.; Whitesides, G. M. *Chem. Phys.* **2002**, *281*, 373.
(49) Parameswaran, R.; Widawsky, J. R.; Vázquez, H.; Park, Y. S.; Boardman, B. M.; Nuckolls, C.; Steigerwald, M. L.; Hybertsen, M. S.; Venkataraman, L. *J. Phys. Chem. Lett.* **2010**, *1*, 2114.
(50) Cheng, Z. L.; Skouta, R.; Vazquez, H.; Widawsky, J. R.; Schneebeli, S.; Chen, W.; Hybertsen, M. S.; Breslow, R.; Venkataraman, L. *Nat. Nanotechnol.* **2011**, *6*, 353.
(51) Hong, W.; Li, H.; Liu, S.-X.; Fu, Y.; Li, J.; Kaliginedi, V.; Decurtins, S.; Wandlowski, T. *J. Am. Chem. Soc.* **2012**, *134*, 19425.

(52) Mishchenko, A.; Zotti, L. A.; Vonlanthen, D.; Bürkle, M.; Pauly, F.; Cuevas, J. C.; Mayor, M.; Wandlowski, T. *J. Am. Chem. Soc.* **2010**, *133*, 184.
(53) Chen, F.; Li, X.; Hihath, J.; Huang, Z.; Tao, N. *J. Am. Chem. Soc.* **2006**, *128*, 15874.
(54) Nerngchamnong, N.; Yuan, L.; Qi, D.-C.; Li, J.; Thompson, D.; Nijhuis, C. A. *Nat. Nanotechnol.* **2013**, *8*, 113.
(55) Wan, A.; Jiang, L.; Sangeeth, C. S. S.; Nijhuis, C. A. *Adv. Fun. Mater.* **2014**, *24*, 4442.
(56) Nijhuis, C. A.; Reus, W. F.; Whitesides, G. M. *J. Am. Chem. Soc.* **2010**, *132*, 18386.
(57) Nijhuis, C. A.; Reus, W. F.; Siegel, A. C.; Whitesides, G. M. *J. Am. Chem. Soc.* **2011**, *133*, 15397.
(58) Nijhuis, C. A.; Reus, W. F.; Barber, J. R.; Dickey, M. D.; Whitesides, G. M. *Nano Lett.* **2010**, *10*, 3611.
(59) Cademartiri, L.; Thuo, M. M.; Nijhuis, C. A.; Reus, W. F.; Tricard, S.; Barber, J. R.; Sodhi, R. N. S.; Brodersen, P.; Kim, C.; Chiechi, R. C.; Whitesides, G. M. *J. Phys. Chem. C* **2012**, *116*, 10848.
(60) Masillamani, A. M.; Crivillers, N.; Orgiu, E.; Rotzler, J.; Bossert, D.; Thippeswamy, R.; Zharnikov, M.; Mayor, M.; Samorì, P. *Chem.—Eur. J.* **2012**, *18*, 10335.
(61) Fracasso, D.; Valkenier, H.; Hummelen, J. C.; Solomon, G. C.; Chiechi, R. C. *J. Am. Chem. Soc.* **2011**, *133*, 9556.
(62) Lorenz, M. R.; Woods, J. F.; Gambino, R. J. *J. Phys. Chem. Solids* **1967**, *28*, 403.
(63) Paterson, G. W.; Wilson, J. A.; Moran, D.; Hill, R.; Long, A. R.; Thayne, I.; Passlack, M.; Droopad, R. *Mater. Sci. Eng., B* **2006**, *135*, 277.
(64) Passlack, M.; Schubert, E. F.; Hobson, W. S.; Hong, M.; Moriya, N.; Chu, S. N. G.; Konstadinidis, K.; Mannaerts, J. P.; Schnoes, M. L.; Zydzik, G. J. *J. Appl. Phys.* **1995**, *77*, 686.
(65) Orita, M.; Ohta, H.; Hirano, M.; Hosono, H. *Appl. Phys. Lett.* **2000**, *77*, 4166.
(66) Ueda, N.; Hosono, H.; Waseda, R.; Kawazoe, H. *Appl. Phys. Lett.* **1997**, *70*, 3561.
(67) Boukamp, B. A. *Solid State Ionics* **1993**, *62*, 131.
(68) Sangeeth, C. S. S.; Jaiswal, M.; Menon, R. *J. Phys.: Condens. Matter* **2009**, *21*, 072101.
(69) Love, J. C.; Estroff, L. A.; Kriebel, J. K.; Nuzzo, R. G.; Whitesides, G. M. *Chem. Rev.* **2005**, *105*, 1103.
(70) Li, C.; Pobelov, I.; Wandlowski, T.; Bagrets, A.; Arnold, A.; Evers, F. *J. Am. Chem. Soc.* **2007**, *130*, 318.
(71) Kockmann, D.; Poelsema, B.; Zandvliet, H. J. W. *Nano Lett.* **2009**, *9*, 1147.
(72) He, H.; Orlando, R.; Blanco, M. A.; Pandey, R.; Amzallag, E.; Baraille, I.; Rerat, M. *Phys. Rev. B: Condens. Matter Mater. Phys.* **2006**, *74*, 195123.
(73) Vilan, A. *J. Phys. Chem. C* **2007**, *111*, 4431.
(74) Vilan, A.; Cahen, D.; Kraisler, E. *ACS Nano* **2012**, *7*, 695.